Chapter 3
Silicene on Ag Substrate

The isolation of graphene sheets from its parent crystal graphite has given the kick to experimental research on its prototypical 2D elemental cousin, silicene (Brumfiel 2013). Unlike graphene, silicene lacks a layered parent material from which it could be derived by exfoliation, as mentioned in Chap. 2. Hence, the efforts of making the silicene dream a reality were focused on epitaxial growth of silicene on substrates. The first synthesis of epitaxial silicene on silver (111) (Vogt et al. 2012; Lin et al. 2012) and zirconium diboride templates (Fleurence et al. 2012) and next on an iridium (111) surface (Meng et al. 2013), has boosted research on other elemental group IV graphene-like materials, namely, germanene and stanene (Matthes et al. 2013; Xu et al. 2013). The boom is motivated by several new possibilities envisaged for future electronics, typically because of the anticipated very high mobilities for silicene and germanene (Ye et al. 2014), as well as potential optical applications (Matthes et al. 2013). It is also fuelled by their predicted robust 2D topological insulator characters (Liu et al. 2011; Ezawa 2012) and potential high temperature superconductor character (Chen et al. 2013; Zhang et al. 2015). One of the most promising candidates as a substrate is Ag because from the studies of the reverse system, where Ag atoms were deposited on silicon substrate, it was known that Ag and silicon make sharp interfaces without making silicide compounds (Le Lay 1983). Indeed, studies on synthesis and characterization of silicene is mainly focused on using Ag(111) as substrates and hence we think it is important to understand this particular system. In this chapter, we present the experimental and theoretical studies investigating the atomic and electronic structure of silicene on Ag substrates.

S. Cahangirov et al., *Introduction to the Physics of Silicene and other 2D Materials*, Lecture Notes in Physics 930,
DOI 10.1007/978-3-319-46572-2_3

3.1 Experimental Evidence

Silicene was synthesized for the first time on Ag (111) substrates (Vogt et al. 2012). Their STM measurements revealed the "flower pattern" (see Fig. 1.2) originating from protruding atoms of 3×3 reconstructed silicene matching the 4×4 supercell of the Ag (111) surface as shown in Fig. 3.1. This structure was also confirmed by

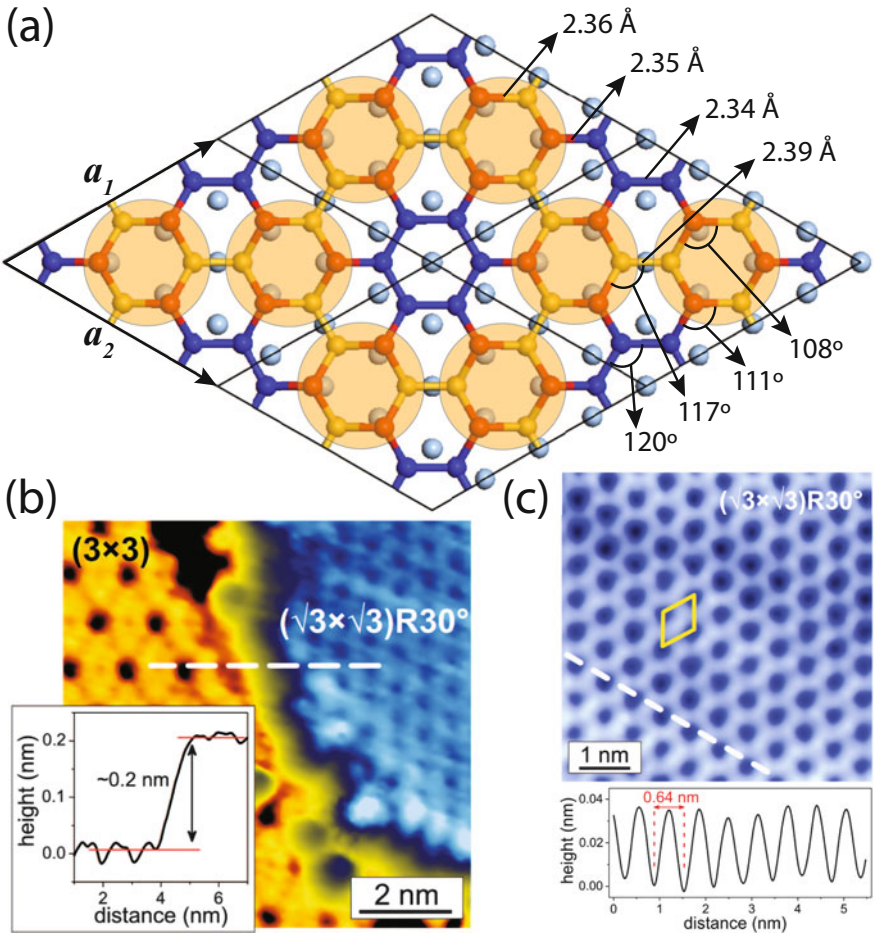

Fig. 3.1 (**a**) *Top view* of 3×3 silicene matched with a 4×4 Ag(111) surface supercell. Only the topmost atomic layer of Ag(111) is shown and represented by *light blue balls*. *Red*, *yellow* and *blue balls* represent Si atoms that are positioned near the top, hollow and the bridge sites of the Ag(111) surface. *Red* Si atoms that are positioned on top of Ag atoms protrude up. *Yellow* Si atoms are mainly interacting with the Ag atoms that sit under the bonds connecting them. When the STM resolution is not high enough, the three protruding *red* Si atoms are seen as a *single dot* represented by transparent *orange circles* drawn around them. These *circles* form large hexagons that have 3×3 periodicity. (**b**) STM image and line profile scanning from 3×3 to $\sqrt{3} \times \sqrt{3}$ silicene on Ag(111). (**c**) STM image and line profile of $\sqrt{3} \times \sqrt{3}$ silicene on Ag(111). Adapted from Vogt et al. (2014)

DFT calculations where the geometry optimization starting from unreconstructed 3×3 supercell of silicene on top of 4×4 supercell of Ag (111) slabs resulted in the reconstructed silicene that reproduced the STM image observed in experiments. Each of these three protrusions seen in STM image make a group of Si atoms that belong to the same silicene sublattice. However, there are two such groups in every 3×3 unitcell that belong to the different sublattices of silicene. This becomes evident when H is deposited on 3×3 silicene which results in a highly asymmetric STM image due to the fact that H atoms prefer to bind only to one of the two sublattices. The atomic structure of 3×3 phase of silicene was also confirmed by reflection high energy positron diffraction (RHEPD) as well as low energy electron diffraction (LEED) experiments (Fukaya et al. 2013; Kawahara et al. 2014). Angle resolved photoemission spectroscopy (ARPES) measurements of the 3×3 silicene phase revealed a linear band starting 0.3 eV below the Fermi level and extending all the way down to −3 eV with a slope of $\sim 1.3 \times 10^6$ m/s (Vogt et al. 2012). This linear band was not detected when silicene was absent. However, the extension and slope of the linear band was too high to be attributed solely to silicene. This created a debate on the origin of these bands that is discussed below.

The archetype single layer silicene, which is the 3×3 phase having a unique orientation, results from a delicate balance between the impinging Si flux (yielding, typically, completion in about 30 min), the surface diffusion of the deposited Si atoms on the bare and silicene covered areas and the competing in-diffusion toward the sub-surface. The growth is driven by these kinetic processes, which, actually, gives a very narrow substrate temperature window of about 200–220 °C (Vogt et al. 2012; Lin et al. 2012). Here silicene forms a highly ordered structure, which can cover 95 % of the crystal surface (Fukaya et al. 2013), because of the exact correspondence between 3 silicene basis vectors and 4 nearest neighbor Ag-Ag distances. The "flower pattern" observed both in STM and non-contact AFM imaging results from the puckered Si atoms sitting nearly on top of Ag atoms, giving a total corrugation of ∼0.07 nm in the silicene sheet (Vogt et al. 2012; Resta et al. 2013).

Already from ∼250 °C a new 2D phase of silicene develops, co-existing with domains of the 3×3/4×4 phase. Since control of the substrate temperature is not easy in this temperature regime where most pyrometers are inoperative and where thermocouples, depending on their locations, generally give improper values, in many cases, mixed 3×3 / 4×4 and $\sqrt{7} \times \sqrt{7}$ / $\sqrt{13} \times \sqrt{13}$ domains are simultaneously observed (Lin et al. 2012). In the latter case, four rotated domains, imposed by symmetry are present, since the $\sqrt{7} \times \sqrt{7}$ silicene domains are rotated by ±19.1° with respect to each of the two $\sqrt{13} \times \sqrt{13}$ Ag super cells, which are themselves rotated by ± 13.9° with respect to the main [−110] and alike directions of the Ag(111) surface. These domains are buckled, differently from the 3×3 / 4×4 case and are accordingly slightly expanded, while remaining commensurate, to accommodate a 4 % reduction in Si coverage ratio (from $\theta_{Si} = 1.125$ for the 3×3 / 4×4 phase to $\theta_{Si} = 1.077$ for this new one), signaling a self-healing process of the silicene mesh, while some of its atoms have disappeared below the surface. These four domains have been imaged simultaneously on the same STM topograph (Resta et al. 2013).

Above about 250 °C, the in-diffusion process is even more active, and, depending on the incident Si flux, a $\sqrt{3} \times \sqrt{3}$ first layer phase may occur, as emphasized by Chen et al., although this has not been reproduced, to the best of our knowledge, by other groups (Chen et al. 2012). Instead, a pseudo "$2\sqrt{3} \times 2\sqrt{3}$" phase is generally obtained (Jamgotchian et al. 2012, 2014; Cinquanta et al. 2013); here, the quotation marks indicate its inherent highly disordered and non-periodic nature resulting from the penetration of Si atoms below the surface (Liu et al. 2014a). Typically, Auger and photoelectron spectroscopy measurements reveal its sudden death, to end, in a dynamic fating process at 300 °C, on the one hand, in multilayer islands through a dewetting mechanism (Acun et al. 2013; Moras et al. 2014; Mannix et al. 2014), and, on the other hand, in the formation of an alloy (Rahman et al. 2015), most probably buried below the surface since the Si LVV signal vanishes in Auger Electron Spectroscopy measurements (Liu et al. 2014a). Finally, we note in passing that a highly perfect, "$(2\sqrt{3} \times 2\sqrt{3}R)30°$ silicene phase", prematurely claimed to have been grown essentially without any defect between 220 and 250 °C (Lalmi et al. 2010; Enriquez et al. 2014), has been proven to be just a delusive phase, i.e., a contrast reversed appearance of the bare Ag(111) surface (Le Lay et al. 2012). At this stage it is worth stressing that both 3×3 / 4×4 and $\sqrt{7} \times \sqrt{7}$ / $\sqrt{13} \times \sqrt{13}$ first layer silicene phases as well as the defected, high temperature "$2\sqrt{3} \times 2\sqrt{3}$" phase, can be encapsulated in situ with an Al_20_3 ultra-thin capping layer. This capping layer, which preserves their integrity, allows for ex situ Raman studies (Cinquanta et al. 2013). It has further permitted the fabrication of the first bottom gate field effect transistor based on a silicene channel (Tao et al. 2015), a clear breakthrough toward device applications (Le Lay 2015).

Unlike the other phases mentioned above, the $\sqrt{3} \times \sqrt{3}$ reconstructed phase of silicene that was observed quite frequently in experiments is not matched by any lattice vector of the Ag (111) substrate (Feng et al. 2012; Chen et al. 2012; Vogt et al. 2014). The $\sqrt{3} \times \sqrt{3}$ reconstructed silicene was first reported by Feng et al. They measured the lattice constant to be 0.64 nm which is ∼5 % less compared to ideal silicene while the STM image was composed of bright triangular spots arranged in a $\sqrt{3} \times \sqrt{3}$ honeycomb lattice (Feng et al. 2012). They have also shown that the same STM image persists in the second layer which hinted that the $\sqrt{3} \times \sqrt{3}$ structure was intrinsic and not formed due to the matching with Ag substrate. Later the $\sqrt{3} \times \sqrt{3}$ reconstruction was also observed in multilayer silicene grown on Ag (111) substrates (Vogt et al. 2014). The distance between consecutive layers was measured to be around 3.0–3.1 Å. Several models were proposed to describe the origin and the atomic structure of the $\sqrt{3} \times \sqrt{3}$ reconstruction. These models are also discussed below.

There are other experimental results worth mentioning. First, this is the ordered adsorption of seven H atoms per unit cell upon in situ exposure of the 3×3/4×4 phase at room temperature to atomic hydrogen (Qiu et al. 2015). This could be a first step toward silicane synthesis; it proves, in any case, the controllable functionalization of silicene, and, possibly opens a route for tuning magnetic properties (Zheng and Zhang 2012). In this sense, one notices that six among these seven H atoms sit on the same triangular silicene sublattice, while the seventh lies

on the other one. Second, it is the observation of large hexagonal patterns with no long range order but remarkable vortices in Low Temperature STM images of triangular $\sqrt{7} \times \sqrt{7}/\sqrt{13} \times \sqrt{13}$ domains (Liu et al. 2014b). We believe that this vortex structure originates due to the stress imposed on silicene upon cooling. Silicene is very likely to have a negative thermal expansion coefficient unlike the silver substrate, exalted by the fact that bulk silicon has such a behavior as well as graphene with the same topology. When cooling, silicene, which is expanded in this phase with respect to the prototype 3×3/4×4 phase, feels too much stress and relaxes it by making vortex-like structures, at variance with the 3×3/4×4 phase which is unchanged down to ∼800 mK.

3.2 Growth Mechanism

The subsequent growth of $\sqrt{3} \times \sqrt{3}$ reconstructed silicene after formation of 3×3 silicene was studied by DFT calculations (Cahangirov et al. 2014b). Here we summarize results of that study. As Si atoms are deposited on Ag(111) surface they search for the optimum structure that minimizes the energy. In the absence of the Ag substrate this optimum structure is the cubic diamond structure that has a cohesive energy of 4.598 eV/atom according to DFT calculations. However, in the presence of the Ag substrate a monolayer of silicene that has primarily 3×3 reconstruction is formed. Here, the 3×3 supercell of silicene is matched with the 4×4 supercell of the Ag(111) surface, as shown in Fig. 3.1a. If we remove the Ag substrate and freeze the Si atoms of the 3×3 reconstructed silicene to calculate its cohesive energy, it turns out to be 3.850 eV/atom, which is 108 meV lower than the buckled freestanding silicene. In fact, if we start from the freestanding 3×3 reconstructed silicene and relax the structure, it goes to the buckled structure, meaning that it is not even a local energy minimum in the absence of the Ag substrate. However, the cohesive energy of 3×3 structure surpasses that of the cubic diamond structure when it is placed on the Ag(111) surface, as seen in Table 3.1. This strong interaction between silicene and the Ag substrate explains the growth of monolayer silicene instead of clustering of Si atoms into bulk structures.

One of the proposed models to explain the growth of the $\sqrt{3} \times \sqrt{3}$ structure is based on the dumbbell structures described in Chap. 2. Note that the 3×3 silicene matches the 4×4 Ag(111) supercell, while the DB structures cannot be matched because their lattice constant is squeezed as the density of DB units is increased as seen in Table 2.1. To include the effect of Ag, the 4×4 Ag (111) slab composed

Table 3.1 Cohesive energies per Si atom and per unit area are given for the 3×3 reconstructed silicene, TDS, LHDS, and HDS structures on the Ag(111) surface

	3 × 3	TDS	LHDS	HDS
Cohesive energy per atom (eV/atom)	4.877	4.663	4.483	4.471
Cohesive energy per area (eV/Å^2)	0.759	0.887	0.938	1.014

of five layers is first squeezed to match the lattice of the 3×3 supercell of the DB structures and then the system is optimized by keeping the Ag atoms fixed. Then the energy of the squeezed Ag substrate in the absence of Si atoms is calculated. The energy difference between these two systems gives the cohesive energies of the DB structures. As seen in Table 3.1, the cohesive energy per Si atom is maximized in the 3×3 silicene while the cohesive energy per area is maximized for the $\sqrt{3}\times\sqrt{3}$ HDS structure. According to the model, when Si atoms are first deposited on Ag (111) substrate, they form the 3×3 reconstructed silicene that has the highest cohesive energy per Si atom, as seen in Table 3.1. At first, the DB units that spontaneously form on 3×3 silicene diffuse and annihilate at the edges and contribute to the growth of even larger 3×3 regions. Once 3×3 silicene reaches sufficiently large area, the DB units compete to form the most energetic structure in a given area covered by 3×3 silicene. To achieve the highest cohesive energy per area, the DB units arrange themselves to form the $\sqrt{3}\times\sqrt{3}$ HDS structure.

The schematic sketch of this growth model is presented in Fig. 3.2a. This picture is in accordance with experiments in which the $\sqrt{3}\times\sqrt{3}$ structure usually appears as islands on top of the first 3×3 silicene layer. As seen in Fig. 3.2b, d, the model also excellently reproduces the distance between $\sqrt{3}\times\sqrt{3}$ and 3×3 surfaces measured to be ∼ 2 Å (Vogt et al. 2014). Furthermore, as shown in Fig. 3.2c, e, the simulated STM image of HDS has the same honeycomb pattern as the one obtained in experiments while the $\sqrt{3}\times\sqrt{3}$ lattice constant of HDS that is calculated to be 6.38 Å, excellently matches the measured value that is ∼6.4 Å (Feng et al. 2012;

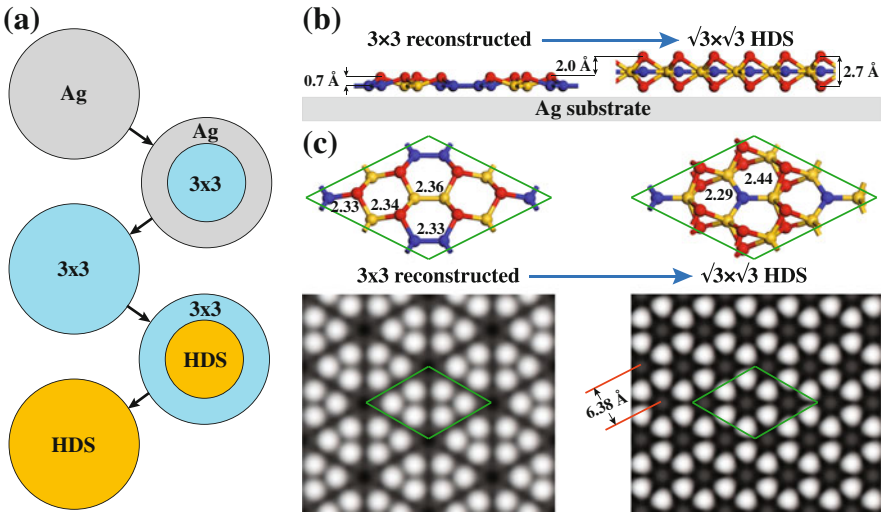

Fig. 3.2 (**a**) Growth sequence of the 3×3 reconstructed silicene and of the HDS structure on the Ag(111) substrate. (**b**) Schematic depiction of the structural transformation from the 3×3 to the $\sqrt{3}\times\sqrt{3}$ reconstruction from the side view. (**c**) Tilted view of the atomic structures and calculated STM images. *Green lozenges* represent the 3×3 supercell

Chen et al. 2012; Vogt et al. 2014). This model can also be extended to explain multilayers that have $\sqrt{3} \times \sqrt{3}$ reconstruction as discussed in Chap. 4 (Cahangirov et al. 2014a).

There are also other proposed models that try to explain the $\sqrt{3} \times \sqrt{3}$ reconstruction. One of them proposes that if monolayer silicene is squeezed enough, then the $\sqrt{3} \times \sqrt{3}$ honeycomb reconstruction becomes energetically more favorable than the ideal 1×1 buckling (Chen et al. 2012). However, this happens if the lattice constant is squeezed down to ∼6.3 Å and also there is no physical reason for the system to remain in this high energy state. Another model is based on the well-studied Si(111)-Ag $\sqrt{3} \times \sqrt{3}$ system (Ding et al. 1991; Shirai et al. 2014). This model also produces a $\sqrt{3} \times \sqrt{3}$ honeycomb pattern in STM measurements. In this case the bright spots are originating from Ag atoms on top of Si(111). However, it is not clear how the 3×3 structure is transformed into $\sqrt{3} \times \sqrt{3}$ structure with Ag atoms on top and also why the lattice is compressed. Further discussion of this model is presented in Chap. 4. Yet another model suggests that the $\sqrt{3} \times \sqrt{3}$ honeycomb STM image is a result of the atomic scale flip-flop motion at the surface of bilayer Si(111) structure formed on top of the 3×3 structure (Guo and Oshiyama 2014). Here the authors suggest that there are three possible configurations and the system is alternating between two of them. Since each state produces a trigonal STM pattern, the combination of two of them should produce the expected honeycomb pattern. However, there is no clear reason why the system should choose to alternate only between two states. Furthermore, this model does not explain the 5 % lattice contraction observed in experiments (Feng et al. 2012; Chen et al. 2012; Vogt et al. 2014).

3.3 The Nature of the Linear Bands

There is no doubt that the linear bands are one of the most intriguing features of silicene. The linear dispersion was observed in 3×3 silicene by ARPES measurements and in $\sqrt{3} \times \sqrt{3}$ silicene by analyzing the quasi-particle interference pattern captured by STM measurements (Vogt et al. 2012; Chen et al. 2012). Both measurements reported very high Fermi velocity of about $1.2 - 1.3 \times 10^6$ m/s. The linear bands were also reported for the multilayer silicene and its ribbons (De Padova et al. 2012, 2013).

The 3×3 reconstruction of silicene forms due to the interaction with the Ag substrate and breaks the symmetry needed to preserve the linearly crossing bands at the Fermi level. This is clearly seen in the band structure of the 3×3 reconstructed silicene isolated from the substrate presented in Fig. 3.3a. Here the band structure of the 3×3 reconstructed silicene is unfolded into the Brillouin zone of the ideal 1×1 silicene. Upon reconstruction, the linearly crossing bands are destroyed and instead there is a 0.3 eV gap at the K point. The scanning tunneling spectroscopy (STS) measurement performed under high magnetic field applied in perpendicular direction to the 3×3 silicene on Ag substrate have shown that the peaks corresponding to the Landau levels corresponding to the presence of the

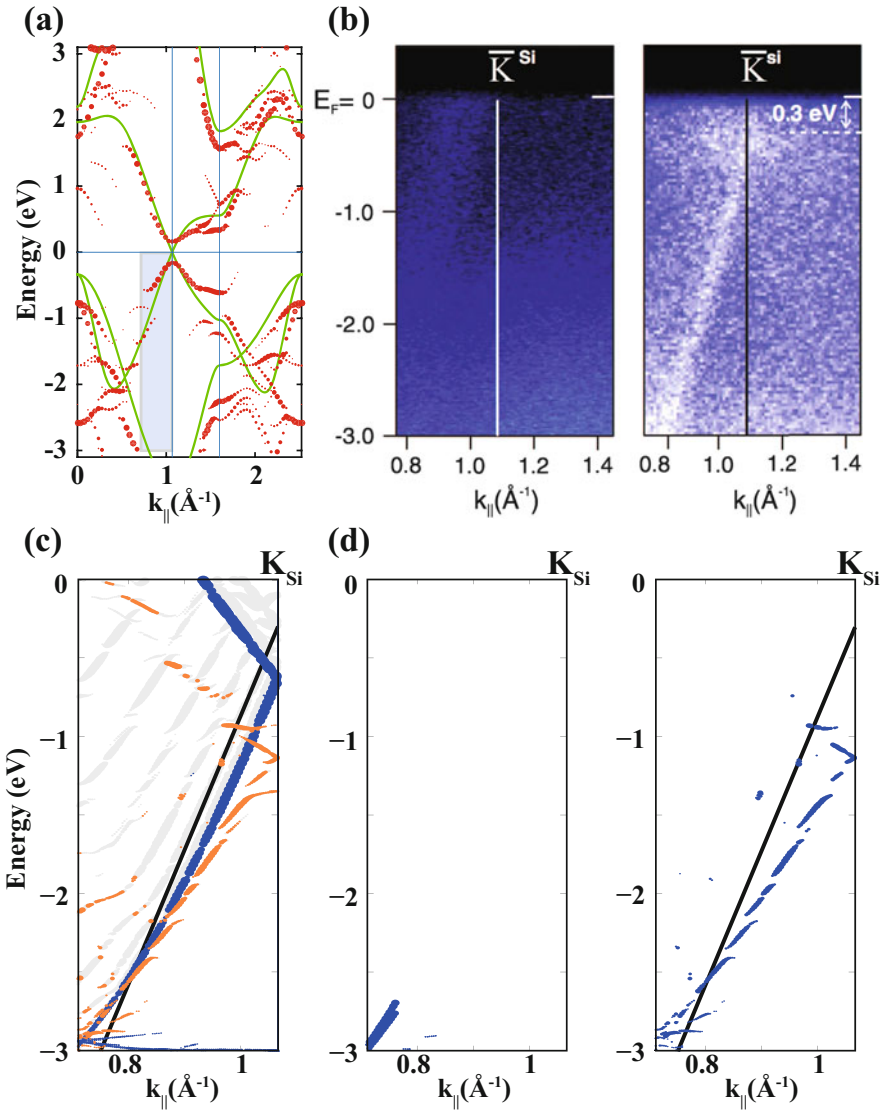

Fig. 3.3 (**a**) Band structure of reconstructed 3×3 silicene (*red dots*) in the absence of Ag substrate unfolded to 1×1 Brillouin zone of silicene. The *dots* radii correspond to the weight of the unfolded state. The band structure of ideally buckled silicene is shown by *green lines*. (**b**) ARPES data around the K point of 1×1 silicene in the absence (*left panel*) and presence (*right panel*) of silicene on Ag(111) substrate [adapted from Vogt et al. (2012)]. (**c**) Band structure of 3×3 silicene a 4×4 Ag(111) 11 layer slab in the experimentally relevant range shown by the *shaded region* in (**a**). The states contributed by 3 Ag layers in the middle of the slab represent the bulk Ag states and are shown by *blue lines*. *Orange lines* are contributed by silicene and 3 Ag layers underneath. The *black line* represents the experimentally observed linear band. (**d**) States contributed by 3 Ag layers underneath silicene in the absence (*left panel*) and presence (*right panel*) of silicene. Adapted from Cahangirov et al. (2013)

Dirac fermions were absent while they were present in the highly oriented pyrolytic graphite samples (Lin et al. 2013). This experimental result was supported by DFT calculations to conclude that Dirac fermions of ideal silicene were destroyed due to the symmetry breaking and hybridization with the Ag substrate.

To interpret the ARPES experiments, Cahangirov et al. calculated the electronic structure of 3×3 silicene placed on top of 11 layers of 4×4 Ag substrate (Cahangirov et al. 2013). Figure 3.3c shows the detailed band structure of the silicene/Ag system in the window where the experiments were performed (see Fig. 3.3b). The blue curve corresponds to the bulk Ag *sp*-band that should not be detected by ARPES which is sensitive to the surface states. Figure 3.3d, e show the states that have significant contribution from surface Ag states when silicene is absent and present, respectively. Here one can choose the threshold in such a way that the linear band disappears when silicene is absent and appears when it is present thereby mimicking the situation observed in ARPES experiments. This analysis suggests that the linear bands are caused by hybridization between silicene and Ag. The perpendicular momentum dependence of the electronic states was calculated by a k-projection technique and was used to calculate the contribution of silicene and Ag to the surface band created by hybridization (Chen and Weinert 2014). This study provided further quantitative agreement with experiments while confirming the hybridized nature of the experimentally observed linear bands. The surface band created by the hybridization between silicene and Ag was detected and distinguished from the faintly visible Ag *sp*-bands in the ARPES measurements (Tsoutsou et al. 2013). There are many other investigations that have reached to conclusion that the linear bands are due to hybridization between silicene and Ag (Guo et al. 2013; Wang and Cheng 2013).

The search for Dirac cones is not limited to the silicene on Ag substrates. ARPES measurements performed on calcium disilicide ($CaSi_2$) revealed a massless Dirac cone located at 2 eV below the Fermi level (Noguchi et al. 2015). $CaSi_2$ can be considered as buckled silicene sandwiched between the planar atomic planes of Ca. The energy shift in the electronic states of silicene is due to significant charge transfer between Si and Ca atoms. First-principles calculations of the $CaSi_2$ structure revealed that there is, in fact, also a momentum shift in the Dirac cone away from the highly symmetric K point (Dutta and Wakabayashi 2015). This is due to the symmetry breaking between the sublattice atoms of silicene and consequent asymmetric interlayer hopping. The shift in the momentum space is also accompanied with a small energy gap opening between the linearly crossing bands.

The Ag substrate plays a crucial role in growth of silicene, as seen from the previous section. This wouldn't be possible if the interaction between silicene and Ag was too weak. A first-principles study of the electronic charge density between silicene and the Ag(111) substrate has concluded that bonds between Si and Ag atoms don't have covalent character (Stephan et al. 2015). However, the strong hybridization with Ag seems to interfere with the delicate electronic structure of silicene, as mentioned above. To avoid this, one has to develop techniques to transfer silicene to less interacting and insulating substrates. Tao et al. have taken an important step in this direction (Tao et al. 2015). They first grew silicene on Ag and

encapsulated it with alumina. Then they flipped the system upside down and etched Ag on silicene, just leaving two Ag pads that they used as metal contacts. In this way they have demonstrated that silicene can operate as an ambipolar field-effect transistor at room temperature.

References

Acun, A., Poelsema, B., Zandvliet, H.J.W., van Gastel, R.: The instability of silicene on Ag(111). Appl. Phys. Lett. **103**, 263119 (2013)

Brumfiel, G.: Sticky problem snares wonder material. Nature **495**, 152–153 (2013)

Cahangirov, S., Audiffred, M., Tang, P., Iacomino, A., Duan, W., Merino, G., Rubio, A.: Electronic structure of silicene on Ag(111): strong hybridization effects. Phys. Rev. B **88**, 035432 (2013)

Cahangirov, S., Özçelik, V.O., Rubio, A., Ciraci, S.: Silicite: The layered allotrope of silicon. Phys. Rev. B **90**, 085426 (2014a)

Cahangirov, S., Özçelik, V.O., Xian, L., Avila, J., Cho, S., Asensio, M.C., Ciraci, S., Rubio, A.: Atomic structure of the $\sqrt{3} \times \sqrt{3}$ phase of silicene on Ag(111). Phys. Rev. B **90**, 035448 (2014b)

Chen, M.X., Weinert, M.: Revealing the substrate origin of the linear dispersion of silicene/Ag(111). Nano Lett. **14**, 5189–5193 (2014)

Chen, L., Liu, C.C., Feng, B., He, X., Cheng, P., Ding, Z., Meng, S., Yao, Y., Wu, K.: Evidence for Dirac fermions in a honeycomb lattice based on silicon. Phys. Rev. Lett. **109**, 056804 (2012)

Chen, L., Feng, B., Wu, K.: Observation of a possible superconducting gap in silicene on Ag(111) surface. Appl. Phys. Lett. **102**, 081602 (2013)

Cinquanta, E., Scalise, E., Chiappe, D., Grazianetti, C., van den Broek, B., Houssa, M., Fanciulli, M., Molle, A.: Getting through the nature of silicene: an sp2-sp3 two-dimensional silicon nanosheet. J. Phys. Chem. C **117**, 16719–16724 (2013)

De Padova, P., Kubo, O., Olivieri, B., Quaresima, C., Nakayama, T., Aono, M., Le Lay, G.: Multilayer silicene nanoribbons. Nano Lett. **12**, 5500–5503 (2012)

De Padova, P., Vogt, P., Resta, A., Avila, J., Razado-Colambo, I., Quaresima, C., Ottaviani, C., Olivieri, B., Bruhn, T., Hirahara, T., Shirai, T., Hasegawa, S., Carmen Asensio, M., Le Lay, G.: Evidence of Dirac fermions in multilayer silicene. Appl. Phys. Lett. **102**, 163106 (2013)

Ding, Y.G., Chan, C.T., Ho, K.M.: Structure of the $(\sqrt{3} \times \sqrt{3})$ $R30°$ Ag/Si(111) surface from first-principles calculations. Phys. Rev. Lett. **67**, 1454–1457 (1991)

Dutta, S., Wakabayashi, K.: Momentum shift of Dirac cones in the silicene-intercalated compound CaSi2. Phys. Rev. B **91**, 201410 (2015)

Enriquez, H., Kara, A., Mayne, A.J., Dujardin, G., Jamgotchian, H., Aufray, B., Oughaddou, H.: Atomic structure of the $(2\sqrt{3} \times 2\sqrt{3}r)30°$ of silicene on Ag(111) surface. J. Phys. Conf. Ser. **491**, 012004 (2014)

Ezawa, M.: Valley-polarized metals and quantum anomalous Hall effect in silicene. Phys. Rev. Lett. **109**, 055502 (2012)

Feng, B., Ding, Z., Meng, S., Yao, Y., He, X., Cheng, P., Chen, L., Wu, K.: Evidence of silicene in honeycomb structures of silicon on Ag(111). Nano Lett. **12**, 3507–3511 (2012)

Fleurence, A., Friedlein, R., Ozaki, T., Kawai, H., Wang, Y., Yamada-Takamura, Y.: Experimental evidence for epitaxial silicene on diboride thin films. Phys. Rev. Lett. **108**, 245501 (2012)

Fukaya, Y., Mochizuki, I., Maekawa, M., Wada, K., Hyodo, T., Matsuda, I., Kawasuso, A.: Structure of silicene on a Ag(111) surface studied by reflection high-energy positron diffraction. Phys. Rev. B **88**, 205413 (2013)

Guo, Z.X., Oshiyama, A.: Structural tristability and deep Dirac states in bilayer silicene on Ag(111) surfaces. Phys. Rev. B **89**, 155418 (2014)

Guo, Z.X., Furuya, S., Iwata, J.I., Oshiyama, A.: Absence and presence of Dirac electrons in silicene on substrates. Phys. Rev. B **87**, 235435 (2013)

Jamgotchian, H., Colignon, Y., Hamzaoui, N., Ealet, B., Hoarau, J.Y., Aufray, B., Bibérian, J.P.: Growth of silicene layers on Ag(111): unexpected effect of the substrate temperature. J. Phys. Condens. Matter **24**, 172001 (2012)

Jamgotchian, H., Colignon, Y., Ealet, B., Parditka, B., Hoarau, J.Y., Girardeaux, C., Aufray, B., Bibérian, J.P.: Silicene on Ag(111) : domains and local defects of the observed superstructures. J. Phys. Conf. Ser. **491**, 012001 (2014)

Kawahara, K., Shirasawa, T., Arafune, R., Lin, C.L., Takahashi, T., Kawai, M., Takagi, N.: Determination of atomic positions in silicene on Ag(111) by low-energy electron diffraction. Surf. Sci. **623**, 25–28 (2014)

Lalmi, B., Oughaddou, H., Enriquez, H., Kara, A., Vizzini, S., Ealet, B., Aufray, B.: Epitaxial growth of a silicene sheet. Appl. Phys. Lett. **97**, 223109 (2010)

Le Lay, G.: Physics and electronics of the noble-metal/elemental-semiconductor interface formation: a status report. Surf. Sci. **132**, 169–204 (1983)

Le Lay, G.: 2D materials: silicene transistors. Nat. Nanotechnol. **10**, 202–203 (2015)

Le Lay, G., Padova, P.D., Resta, A., Bruhn, T., Vogt, P.: Epitaxial silicene: can it be strongly strained? J. Phys. D. Appl. Phys. **45**, 392001 (2012)

Lin, C.L., Arafune, R., Kawahara, K., Tsukahara, N., Minamitani, E., Kim, Y., Takagi, N., Kawai, M.: Structure of silicene grown on Ag(111). Appl. Phys. Express **5**, 045802 (2012)

Lin, C.L., Arafune, R., Kawahara, K., Kanno, M., Tsukahara, N., Minamitani, E., Kim, Y., Kawai, M., Takagi, N.: Substrate-induced symmetry breaking in silicene. Phys. Rev. Lett. **110**, 076801 (2013)

Liu, C.C., Feng, W., Yao, Y.: Quantum spin Hall effect in silicene and two-dimensional germanium. Phys. Rev. Lett. **107**, 076802 (2011)

Liu, Z.L., Wang, M.X., Liu, C., Jia, J.F., Vogt, P., Quaresima, C., Ottaviani, C., Olivieri, B., De Padova, P., Lay, G.L.: The fate of the $2\sqrt{3}\times2\sqrt{3}$r(30°) silicene phase on Ag(111). APL Mater. **2**, 092513 (2014a)

Liu, Z.L., Wang, M.X., Xu, J.P., Ge, J.F., Lay, G.L., Vogt, P., Qian, D., Gao, C.L., Liu, C., Jia, J.F.: Various atomic structures of monolayer silicene fabricated on Ag(111). New J. Phys. **16**, 075006 (2014b)

Mannix, A.J., Kiraly, B., Fisher, B.L., Hersam, M.C., Guisinger, N.P.: Silicon growth at the two-dimensional limit on Ag(111). ACS Nano **8**, 7538–7547 (2014)

Matthes, L., Pulci, O., Bechstedt, F.: Massive Dirac quasiparticles in the optical absorbance of graphene, silicene, germanene, and tinene. J. Phys. Condens. Matter **25**, 395305 (2013)

Meng, L., Wang, Y., Zhang, L., Du, S., Wu, R., Li, L., Zhang, Y., Li, G., Zhou, H., Hofer, W.A., Gao, H.J.: Buckled silicene formation on Ir(111). Nano Lett. **13**, 685–690 (2013)

Moras, P., Mentes, T.O., Sheverdyaeva, P.M., Locatelli, A., Carbone, C.: Coexistence of multiple silicene phases in silicon grown on Ag(111). J. Phys. Condens. Matter **26**, 185001 (2014)

Noguchi, E., Sugawara, K., Yaokawa, R., Hitosugi, T., Nakano, H., Takahashi, T.: Direct observation of Dirac cone in multilayer silicene intercalation compound CaSi2. Adv. Mater. **27**, 856–860 (2015)

Qiu, J., Fu, H., Xu, Y., Oreshkin, A.I., Shao, T., Li, H., Meng, S., Chen, L., Wu, K.: Ordered and reversible hydrogenation of silicene. Phys. Rev. Lett. **114**, 126101 (2015)

Rahman, M.S., Nakagawa, T., Mizuno, S.: Growth of Si on Ag(111) and determination of large commensurate unit cell of high-temperature phase. Jpn. J. Appl. Phys. **54**, 015502 (2015)

Resta, A., Leoni, T., Barth, C., Ranguis, A., Becker, C., Bruhn, T., Vogt, P., Le Lay, G.: Atomic structures of silicene layers grown on Ag(111): scanning tunneling microscopy and noncontact atomic force microscopy observations. Sci. Rep. **3** (2013)

Shirai, T., Shirasawa, T., Hirahara, T., Fukui, N., Takahashi, T., Hasegawa, S.: Structure determination of multilayer silicene grown on Ag(111) films by electron diffraction: evidence for Ag segregation at the surface. Phys. Rev. B **89**, 241403 (2014)

Stephan, R., Hanf, M.C., Sonnet, P.: Spatial analysis of interactions at the silicene/Ag interface: first principles study. J. Phys. Condens. Matter **27**, 015002 (2015)

Tao, L., Cinquanta, E., Chiappe, D., Grazianetti, C., Fanciulli, M., Dubey, M., Molle, A., Akinwande, D.: Silicene field-effect transistors operating at room temperature. Nat. Nanotechnol. **10**, 227–231 (2015)

Tsoutsou, D., Xenogiannopoulou, E., Golias, E., Tsipas, P., Dimoulas, A.: Evidence for hybrid surface metallic band in (4?×?4) silicene on Ag(111). Appl. Phys. Lett. **103**, 231604 (2013)

Vogt, P., De Padova, P., Quaresima, C., Avila, J., Frantzeskakis, E., Asensio, M.C., Resta, A., Ealet, B., Le Lay, G.: Silicene: Compelling experimental evidence for graphenelike two-dimensional silicon. Phys. Rev. Lett. **108**, 155501 (2012)

Vogt, P., Capiod, P., Berthe, M., Resta, A., De Padova, P., Bruhn, T., Le Lay, G., Grandidier, B.: Synthesis and electrical conductivity of multilayer silicene. Appl. Phys. Lett. **104**, 021602 (2014)

Wang, Y.P., Cheng, H.P.: Absence of a Dirac cone in silicene on Ag(111): First-principles density functional calculations with a modified effective band structure technique. Phys. Rev. B **87**, 245430 (2013)

Xu, Y., Yan, B., Zhang, H.J., Wang, J., Xu, G., Tang, P., Duan, W., Zhang, S.C.: Large-gap quantum spin Hall insulators in tin films. Phys. Rev. Lett. **111**, 136804 (2013)

Ye, X.S., Shao, Z.G., Zhao, H., Yang, L., Wang, C.L.: Intrinsic carrier mobility of germanene is larger than graphene's: first-principle calculations. RSC Adv. **4**, 21216–21220 (2014)

Zhang, L.D., Yang, F., Yao, Y.: Possible electric-field-induced superconducting states in doped silicene. Sci. Rep. **5**, 8203-1–8203-6 (2015)

Zheng, F.B., Zhang, C.w.: The electronic and magnetic properties of functionalized silicene: a first-principles study. Nanoscale Res. Lett. **7**, 422 (2012)